Available online at www.sciencedirect.com
ScienceDirect
Journal of Nuclear Materials 373 (2008) 343–350
journal of nuclear materials
www.elsevier.com/locate/jnucmat

Corrosion and oxide characteristics of Zr–1.5Nb–0.4Sn–0.2Fe–0.1Cr alloys in 360 °C pure water and LiOH solution

Jeong-Yong Park *, Seung Jo Yoo, Byung-Kwon Choi, Yong Hwan Jeong

Advanced Core Materials Laboratory, Korea Atomic Energy Research Institute, 150 Deokjin-dong, Yuseong-gu, Daejeon 305–353, Republic of Korea

Received 21 December 2006; accepted 2 June 2007

Abstract

Corrosion behavior of Zr–1.5Nb–0.4Sn–0.2Fe–0.1Cr (HANA-4) and Zircaloy-4 was investigated in 360 °C pure water and in 360 °C water containing 70 ppm Li. HANA-4 showed a much better corrosion resistance than Zircaloy-4 in pure water and maintained a lower corrosion rate even in LiOH solution where Zircaloy-4 showed an accelerated corrosion behavior. The oxide was characterized by an optical microscopy and a transmission electron microscopy. The oxide formed on HANA-4 in pure water was observed to have a layered structure with a smaller total oxide thickness for the same corrosion period, a higher layer thickness and a larger columnar grain size in the interface region when compared to Zircaloy-4. The oxide protectiveness of HANA-4 was also effective in maintaining a lower corrosion rate even in LiOH solution where a layered structure was not developed in the oxide of Zircaloy-4. This demonstrates that the oxide of HANA-4 was protective enough to prevent it from becoming porous by an ingress of Li^+ or LiOH.

1. Introduction

Waterside corrosion of fuel claddings has been considered as one of the main limitations to a burn-up extension of a nuclear fuel and a key issue in improving the economical efficiency of light water reactors (LWRs). Since Zr alloys are used as fuel claddings, advanced Zr alloys have been developed continuously with a focus on an improvement of the corrosion resistance. Recently, a series of Nb-containing Zr alloys named HANA has been developed to improve the corrosion resistance of the fuel claddings on the basis of the correlations between the corrosion behavior and the metallurgical factors including the chemical composition, the microstructure and the precipitate characteristics [1]. HANA alloys exhibited an excellent corrosion resistance in the out-reactor as well as the in-reactor conditions when compared to Zircaloy-4 [1].

Even though the empirical correlation of the corrosion behavior and the metallurgical factors are well established for Zr alloys, the corrosion mechanism is not fully understood even for Zircaloy-4. Moreover, the corrosion mechanism of Nb-containing Zr alloys is likely to be governed by a different mechanism from that of Zircaloy-4. Like other Nb-containing Zr alloys such as ZIRLO [2] and M5 [3], the corrosion mechanism of HANA alloys was not fully clarified even though it has been confirmed that the addition of Nb was very effective to reduce the corrosion rate of Zr alloys [1,4]. On the other hand, Nb-containing Zr alloys behave differently in LiOH solution where Zircaloy-4 shows an accelerated corrosion behavior. LiOH has been added into a coolant to control the pH and thereby preventing the formation of CRUD which might cause an activity problem during a reactor operation. Therefore, it is crucial to investigate the corrosion behavior of newly-developed Zr alloys such as HANA in LiOH solution.

This investigation is a part of a systematic study to examine the corrosion behavior and oxide properties of HANA alloys and it aims at contributing to the understanding on

* Corresponding author. Tel.: +82 42 868 8911; fax: +82 42 862 0432.
E-mail address: parkjy@kaeri.re.kr (J.-Y. Park).

0022-3115/$ - see front matter © 2007 Elsevier B.V. All rights reserved.
doi:10.1016/j.jnucmat.2007.06.015

the corrosion mechanism of Nb-containing Zr alloys. In this study, the corrosion behavior of the HANA alloys was investigated and compared with Zircaloy-4 in 360 °C water and in 360 °C water containing 70 ppm Li. Since a lack of an understanding on the corrosion mechanism is thought to be partly due to an insufficient oxide characterization, the oxides formed during the corrosion tests were systematically characterized to clarify the reason why Nb-containing Zr alloys including HANA alloys exhibited an improved corrosion resistance.

2. Experimental procedure

The chemical compositions of the Zr alloys used in this study are shown in Table 1. The two main differences in the chemical compositions between two alloys are the addition of Nb and the smaller Sn concentration in HANA-4 when compared to Zircaloy-4 while the contents of Fe and Cr are identical in the two alloys. HANA-4 was manufactured as tubes with an outer diameter of 9.5 mm and a wall thickness of 0.57 mm. The final annealing for HANA-4 tubes was performed at 470 °C for 8 h. On the other hand, the commercial Zircaloy-4 tubes were used in an as-received state as a reference. The as-received Zircaloy-4 was reported to be subjected to the final heat-treatment at 475 °C for 3–8 h.

Corrosion tests were performed by using autoclaves for 1020 days in 360 °C pure water and for 830 days in 360 °C water containing 70 ppm Li. The deionized water was used for pure water environment and the LiOH solution was prepared to make Li concentration of 70 ppm by mixing LiOH in the deionized water. The pH of the LiOH solution was calculated to be 10.17 at 360 °C. Before starting the corrosion test, the water in the autoclave was blown with Ar gas to lower the dissolved oxygen concentration. The corrosion test specimens were cut into the segment tubes with a length of 40 mm for HANA-4 and 30 mm for Zircaloy-4 and then pickled in a solution of 10 vol.% HF, 30 vol.% H_2SO_4, 30 vol.% HNO_3 and 30 vol.% H_2O. Four corrosion specimens for each alloy were employed in the corrosion test. The corrosion behavior was evaluated by measuring the weight gain of the corrosion test specimens which were periodically taken out of the autoclaves. The representative weight gain of the alloy was obtained by averaging the measured values from the four corrosion specimens.

The oxides formed on the corrosion test specimens were characterized by a reflected and transmitted light optical microscopy and a transmission electron microscopy (TEM). The samples for the reflected optical microscopy were prepared by cutting the corroded tube and polishing the cross-section on the SiC paper with a grit number 4000. In order to observe the cross-section of the oxide by a transmitted light optical microscopy (TLOM) and TEM, the corroded tube specimens were sliced to have a thickness of 300 μm and then thinned to a thickness of less than 20 μm by a mechanical polishing of the cross section of the samples. Finally, the thinned samples were ion-milled by using Fishione Lamp 1010 for TLOM and by a focused ion beam using NOVA 600 for TEM. The grain morphology of the oxide and the incorporated precipitates were examined by TEM. The types of precipitates in the oxide were identified by analyzing the selected area diffraction pattern (SADP) and the chemical composition from the energy dispersive X-ray spectroscopy (EDS).

Table 1
Nominal compositions of the Zr alloys used in this study (wt%)

Alloy	Nb	Sn	Fe	Cr
HANA-4	1.5	0.4	0.2	0.1
Zircaloy-4		1.3	0.2	0.1

3. Results and discussion

3.1. Corrosion properties

Fig. 1 shows the corrosion behavior of HANA-4 and Zircaloy-4 in 360 °C pure water and in 360 °C water containing 70 ppm Li. HANA-4 showed a much better corrosion resistance than Zircaloy-4 in both corrosion environments. The corrosion rates were calculated on the

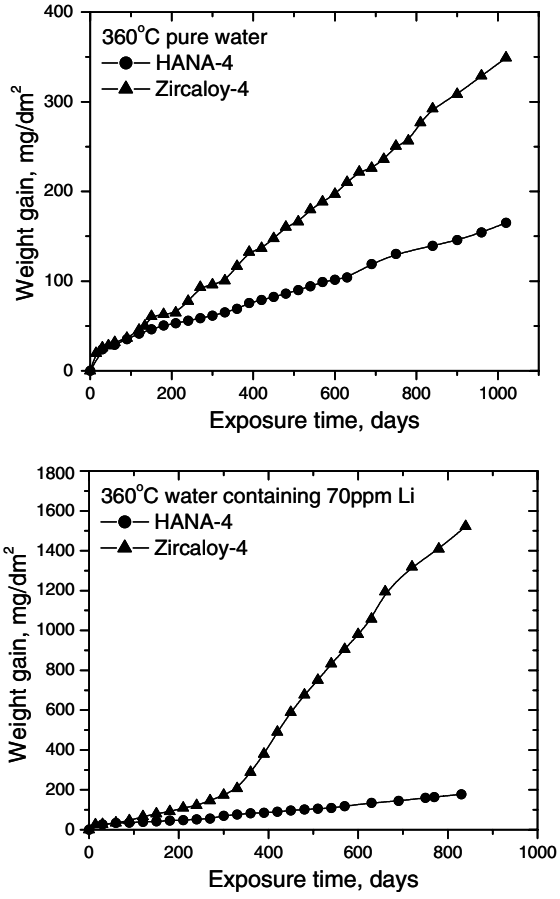

Fig. 1. Corrosion behavior of HANA-4 and Zircaloy-4 in 360 °C pure water and in 360 °C water containing 70 ppm Li.

Table 2
Characteristics of the corrosion behavior and the oxide layer structure

Alloy	Corrosion environment[a]	Exposure time (days)	Corrosion rate[b] (mg dm^{-1} d^{-1})	Total oxide thickness (μm)	No. of layer	Thickness of fully eveloped layer (μm)	Thickness of developing layer (μm)
HANA-4	Pure water	1020	0.14	10.3	3	2.9	1.6
	70 ppm Li	830	0.19	14.3	5	2.6	1.3
Zircaloy-4	Pure water	1020	0.33	18.3	7	2.4	1.5
	70 ppm Li	830	0.54/2.65[c]	65.6	–	–	–

[a] Corrosion tests were performed at 360 °C by using autoclaves.
[b] Corrosion rate was calculated on the basis on the linear regression to the long-term corrosion data.
[c] Corrosion rate was calculated in two regimes which were separated by the breakaway.

basis on the linear regression to the long-term corrosion data. The calculated corrosion rates were shown in Table 2. The corrosion rate of HANA-4 was only slightly increased even though the corrosion environment was changed from pure water to LiOH solution. The corrosion rate of Zircaloy-4 was more than 2 times higher than that of HANA-4 in pure water. In LiOH solution, however, Zircaloy-4 showed an accelerated corrosion behavior after 330 days. The corrosion rate was increased by approximately 5 times after the transition point and it was 14 times faster than that of HANA-4.

HANA-4 was found to have two types of precipitates which were β-Nb with a bcc crystal structure and $Zr(Nb, Fe, Cr)_2$ with a hcp structure. Such a microstructure was not changed even after 1020 days of corrosion test. Regarding the effect of the alloying element on the corrosion properties of Zr alloys, the addition of Nb has already been confirmed to be beneficial in many previous studies [1–4]. It has also been reported that the corrosion resistance of Zr alloys was increased with a decrease of Sn content [5]. In this study, the synergetic effect of the addition of Nb and the reduction of Sn might be achieved in HANA-4 when compared to Zircaloy-4, although it was hard to determine which effect was more significant in the improvement of the corrosion resistance. Moreover, such a beneficial effect was even more remarkable in LiOH solution where a corrosion acceleration of Zircaloy-4 was generally observed.

3.2. Oxide/metal interface morphology by OM

After the corrosion tests, the cross-sections of the oxides were observed by a reflected light optical microscopy to examine the interface morphology. Fig. 2 shows the cross-sections of the oxide formed on HANA-4 and Zircaloy-4 which were corroded for 1020 days in pure water and for 830 days in LiOH solution. The oxide/metal interface was shown to be flat in HANA-4 regardless of the corrosion conditions. However, Zricaloy-4 was shown to have

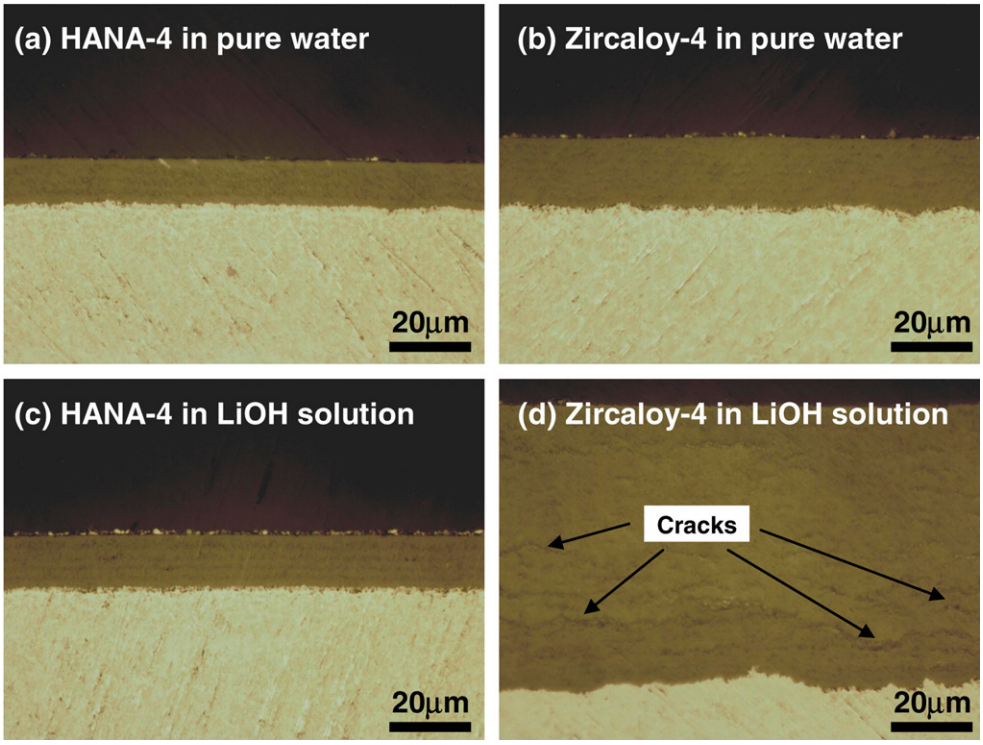

Fig. 2. Reflected light optical micrographs of the oxides formed on ((a),(c)) HANA-4 and ((b),(d)) Zircaloy-4 in ((a),(b)) 360 °C pure water for 1020 days and in ((c),(d)) 360 °C water containing 70 ppm Li for 830 days.

a relatively irregular and wavy interface even in the pure water condition where the corrosion rate was relatively low. Moreover, a number of lateral cracks were also observed especially in the oxide on Zircaloy-4 in LiOH solution. It was revealed that the interface was more irregular in the alloy exhibiting a higher corrosion rate. However, it is not clear whether the irregular interface is one of the root causes for the higher corrosion rate of Zircaloy-4 even though an irregular interface is thought to be closely related to the inhomogeneous stress build-up during an oxide growth [6].

3.3. Oxide structure by TLOM

Fig. 3 shows the transmitted light optical micrographs of the oxides which were formed on HANA-4 and Zircaloy-4 in 360 °C pure water. The oxide was found to consist of many layers regardless of the alloy compositions. In the same oxide, the thickness of the layer was almost identical except that the layer adjacent to the oxide/metal interface was thinner than the other layers because it was still growing. This result is in good agreement with a previous observation by Yilmazbayhan et al. [7]. The layered structure of the oxide seen in TLOM is attributed to the fact that the oxide microstructure was changed periodically during the oxide growth [8] and closely related to the cyclic nature of the corrosion kinetics [9]. It is noteworthy that the thickness of the fully developed layer, i.e., the average layer thickness except for the layer bordering the interface, was higher in the oxide of HANA-4 showing a lower total oxide thickness due to the lower corrosion rate. It implies that the oxide of HANA-4 could grow thicker before the transition when compared to that of Zircaloy-4. The frequent transition of the oxide growth would make the oxide more susceptible to a diffusion of the oxygen ions since the transition was accompanied by a re-nucleation of the equiaxed grains [8]. Therefore, a higher layer thickness would be the one of the main reasons why HANA-4 showed a better corrosion resistance when compared to Zircaloy-4.

A layered structure was also shown in the oxide formed in LiOH solution especially for HANA-4 even though the layer thickness was decreased a little in LiOH condition as shown in Fig. 4. However, the layered structure was not able to be defined in the oxide of Zircaloy-4 showing a breakaway corrosion behavior in LiOH solution. A vertical crack was also shown to penetrate from the surface to the long lateral crack near the oxide/metal interface, which would act as the direct path that the oxidizing species can reach the interface more readily. The vertical cracks, however, did not form periodically though their formation is observed only in the oxide of Zircaloy-4 in LiOH solution. It was revealed that the oxide on HANA-4 maintained its protective nature even in LiOH solution. This is in good agreement with a previous observation where ZIRLO was shown to have an oxide consisting of well-defined layers while Zircaloy-4 had no layered structure in the oxide after a corrosion test in LiOH solution

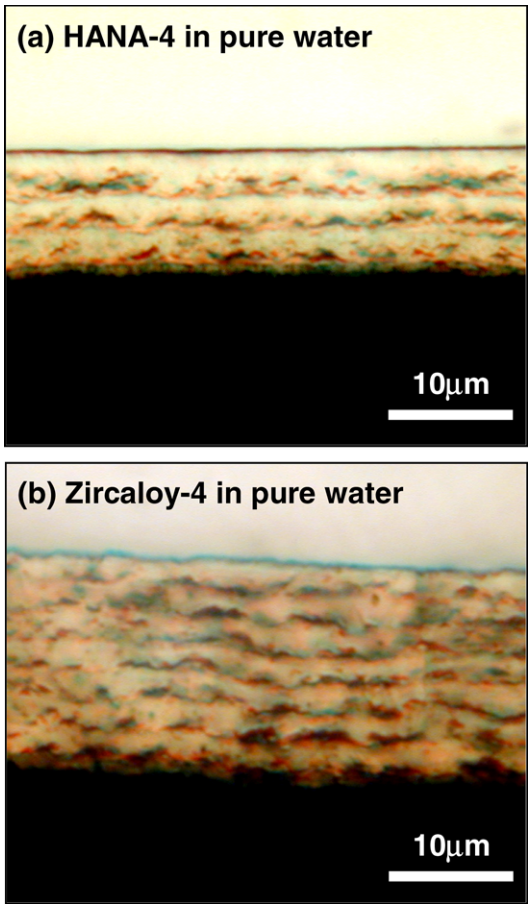

Fig. 3. Transmitted light optical micrographs of the oxides on (a) HANA-4 and (b) Zircaloy-4 corroded in 360 °C pure water for 1020 days.

[8]. The oxide layer structure observed by TLOM was summarized in Table 2. The total oxide thickness and the number of layers were higher in the alloys showing a higher corrosion rate. However, the thickness of the fully developed layer was higher in the alloy showing a lower corrosion rate. It is noted here that a layered structure was not developed in the oxide whose growth rate was very high. This seems to be due to the fact that equiaxed grains are predominant in a fast growing oxide rather than a periodic change of the grain morphology.

3.4. Grain morphology by TEM

Fig. 5 shows the grain morphology in the interface region of the oxide on HANA-4 which was corroded for 1020 days in 360 °C pure water (Fig. 5(a)) and for 830 days in LiOH solution (Fig. 5(b)). The oxide in the interface region mainly consisted of columnar grains whose size were 200–300 nm in length and 20–50 nm in width. The columnar grain size in the oxide of HANA-4 was almost similar in both corrosion environments. Some cracks are also observed in the interface region of the oxide formed in pure water. The internal stress accumulated during an oxide growth would be relieved with a crack formation. In Fig. 5, however, it is not clear if the cracks are originated

from the stress relieving process or they are artifacts of the sample preparation. Zircaloy-4 corroded in pure water also had columnar oxide grains in the interface region as shown in Fig. 6(a). However, the size of the columnar grain was smaller in Zircaloy-4 when compared to HANA-4. The columnar grain size in the oxide of Zircaloy-4 was changed from 150 to 250 nm in length and from 20 to 40 nm in width in pure water but it was not able to be defined in LiOH solution as shown in Fig. 6(b). Columnar grains are more desirable to retard the diffusion rate of the oxygen ions when compared to the equiaxed grains since the oxygen ions move through a grain boundary of the oxide. Such a beneficial effect would be enhanced if the grain size of the columnar grain is increased. Therefore, along with the higher thickness of the layer, the larger columnar oxide grains were considered as one of the reasons for the lower corrosion rate of HANA-4.

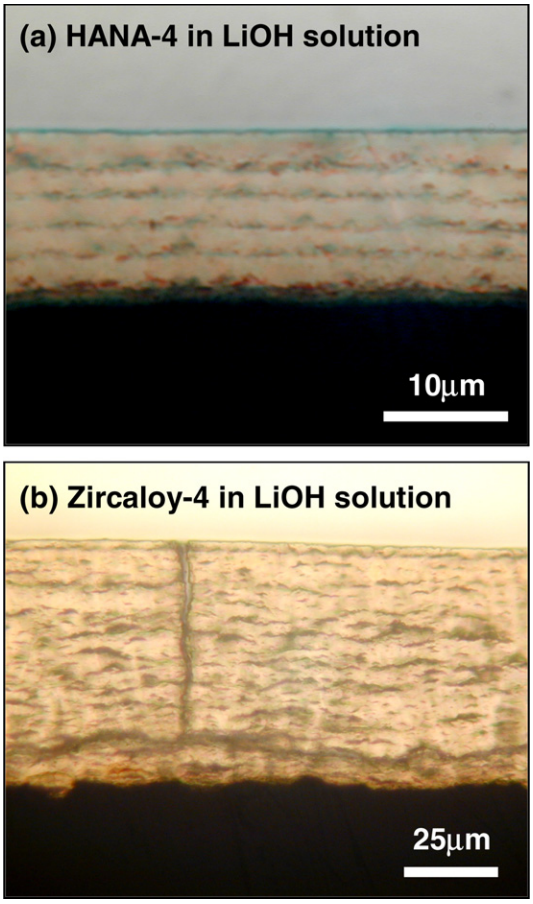

Fig. 4. Transmitted light optical micrographs of the oxides on (a) HANA-4 and (b) Zircaloy-4 corroded in 360 °C water containing 70 ppm Li for 830 days.

In this study, the alloy showing a lower corrosion rate was found to have a layered structure of the oxide with a smaller total oxide thickness for the same period of an oxidation, a higher layer thickness and a larger columnar grain size. The layer thickness would be indicative of the critical thickness that the oxide can withstand for the accumulated stress before the transition during an oxide grain growth. It was revealed in this study that the layer thickness was higher in the oxide with larger columnar grains, i.e., a lower corrosion rate of the oxygen ions.

The difference in the columnar grain size between HANA-4 and Zircaloy-4 is likely to be attributed to the difference in the alloying element. It has been reported that Sn is responsible for the degradation of oxide protectiveness in Zr alloys [5]. During the oxidation process, Sn is segregated in the grain boundary of ZrO_2 and then oxidized lately to form SnO or Sn_3O_4 [5]. The existence of a metallic Sn in a pre-transition oxide was also observed by using a Mossbauer spectroscopy by Pecheur et al. [10]. Such a late oxidation of Sn would inhibit the columnar

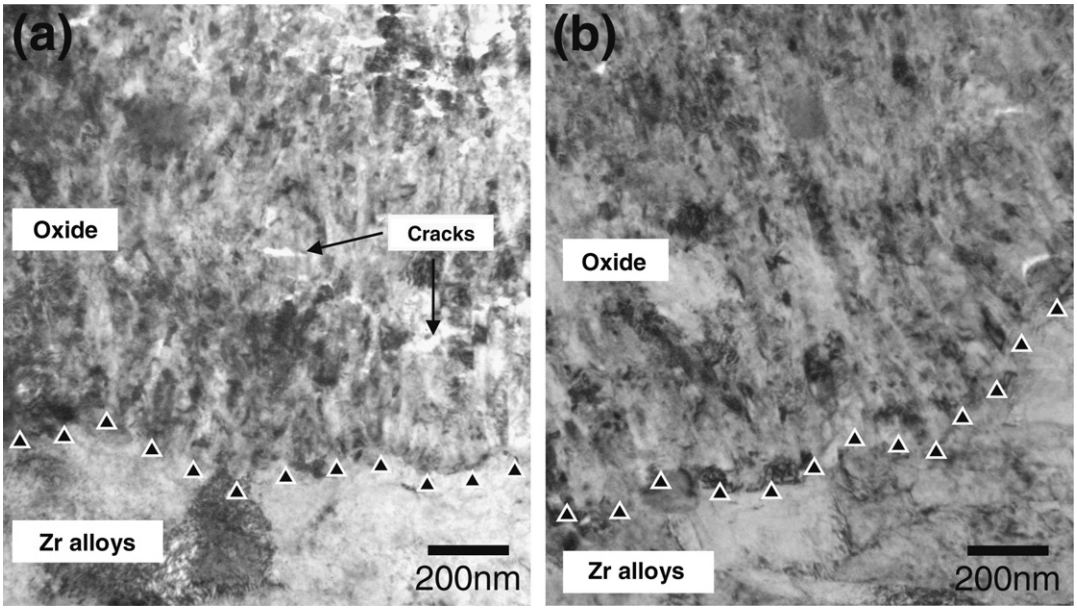

Fig. 5. Grain morphology of the interface region of the oxide on HANA-4 corroded in (a) 360 °C pure water for 1020 days and in (b) 360 °C water containing 70 ppm Li for 830 days.

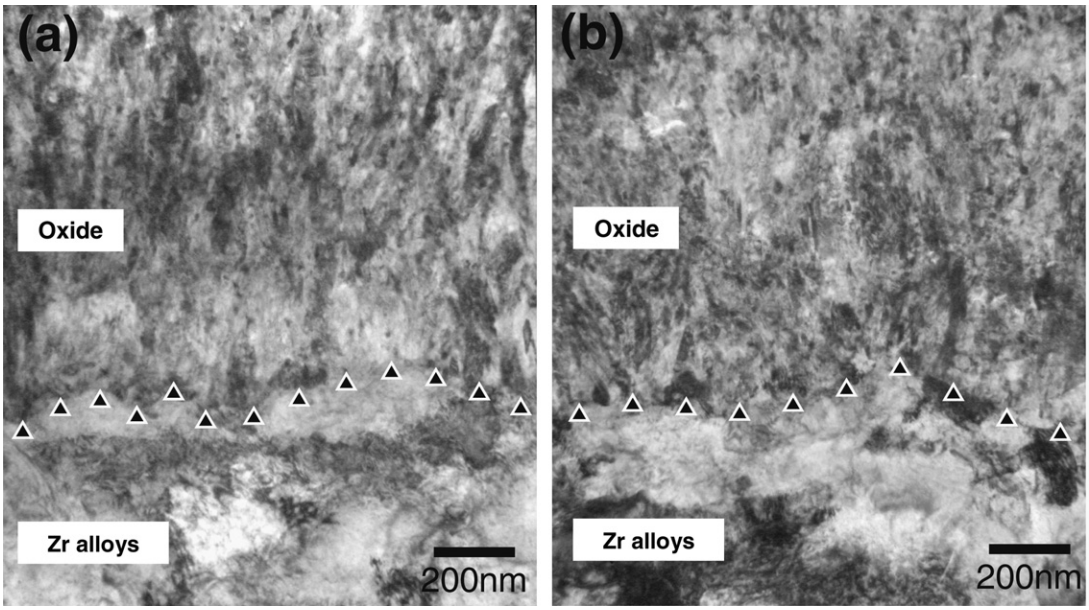

Fig. 6. Grain morphology of the interface region of the oxide formed on Zircaloy-4 corroded in (a) 360 °C pure water for 1020 days and in (b) 360 °C water containing 70 ppm Li for 830 days.

grain growth and promote a renucleation of the equiaxed grains and in turn lead to an increase of the corrosion rates. Gebhardt et al. observed that the fraction of the equiaxed grains in the oxide was increased with an increase of Sn content [11]. It is thought that the larger columnar grains observed in the oxide of HANA-4 were partly related to a reduction of the Sn effect on an oxide grain growth.

On the other hand, the addition of Nb is known to be very effective in increasing the corrosion resistance of Zr alloys. The role of Nb would be different from that of Sn in the process of an oxide growth of HANA-4 since most of Nb are in the form of the precipitates such as β-Nb or $Zr(Nb,Fe,Cr)_2$ whereas Sn exist as solute elements. It has been reported that a fine distribution of β-Nb is the main reason for the good corrosion resistance of ZIRLO [12]. However, it is not well understood how the precipitates, which were incorporated into the oxide, affect the grain morphology of the oxide. Based on the comparison of HANA-4 with Zircaloy-4, it was revealed that the reduction of Sn concentration and the addition of Nb are the main reasons for the formation of the protective oxide, thereby improving the corrosion resistance of HANA-4. However, it was difficult to clarify which effect is more dominant since the effect of Sn reduction and Nb addition was not examined separately in this study.

3.5. Precipitates incorporated into the oxide

Precipitates of the Zr alloys are generally considered as the key parameter that explains the relationship between the microstructure and the corrosion behavior of Zr alloys [12–14]. Since the precipitates are oxidized later than the matrix, the oxide properties would be influenced by a late oxidation. The characteristics of a late oxidation of the incorporated precipitates would exert a significant impact on the existing oxide, which would be different depending on the precipitate characteristics.

Fig. 7(a) shows the incorporated $Zr(Fe,Cr)_2$ precipitate at about 3.5 μm away from the oxide/metal interface of Zircaloy-4 which was corroded for 1020 days in pure water. The precipitate was oxidized and changed to a number of nanocrystallites. In the vicinity of the oxidized precipitate, we also observed cracks which were thought to be induced by an oxidation of the precipitate. This result is in good agreement with the previous observation on an oxidized $Zr(Fe,Cr)_2$ in Zircaloy-4 by Pecheur et al. [13]. This type of a late oxidation would increase the corrosion rate by making the oxide more susceptible to the diffusion of a oxygen ion. Anada et al. reported that a transformation from columnar grains to equiaxed grains was observed dominantly around the oxidized precipitates and the oxidation of the precipitates was the cause of an accelerated corrosion [14].

The oxidation characteristics of the precipitates in HANA-4 were different from that of Zircaloy-4. Fig. 7(b) shows the incorporated $Zr(Nb,Fe,Cr)_2$ at about 3.5 μm from the oxide/metal interface of HANA-4 corroded for 1020 days in pure water. It was revealed from SADP and EDS results that the precipitate was oxidized and amorphized. It was also found that β-Nb was oxidized in a similar manner with $Zr(Nb,Fe,Cr)_2$. Lin et al. observed that β-Nb exhibited a delayed oxidation with respect to α-Zr, forming a metallic sub-oxide initially and becoming amorphous when oxidized [15]. However, we were not able to observe nanocrystallites and cracks in the oxide of HANA-4 when the precipitate was oxidized. Such an oxidation behavior of the incorporated precipitates would be desirable in terms of an oxide protectiveness by preventing the oxide from becoming porous. Therefore it is suggested

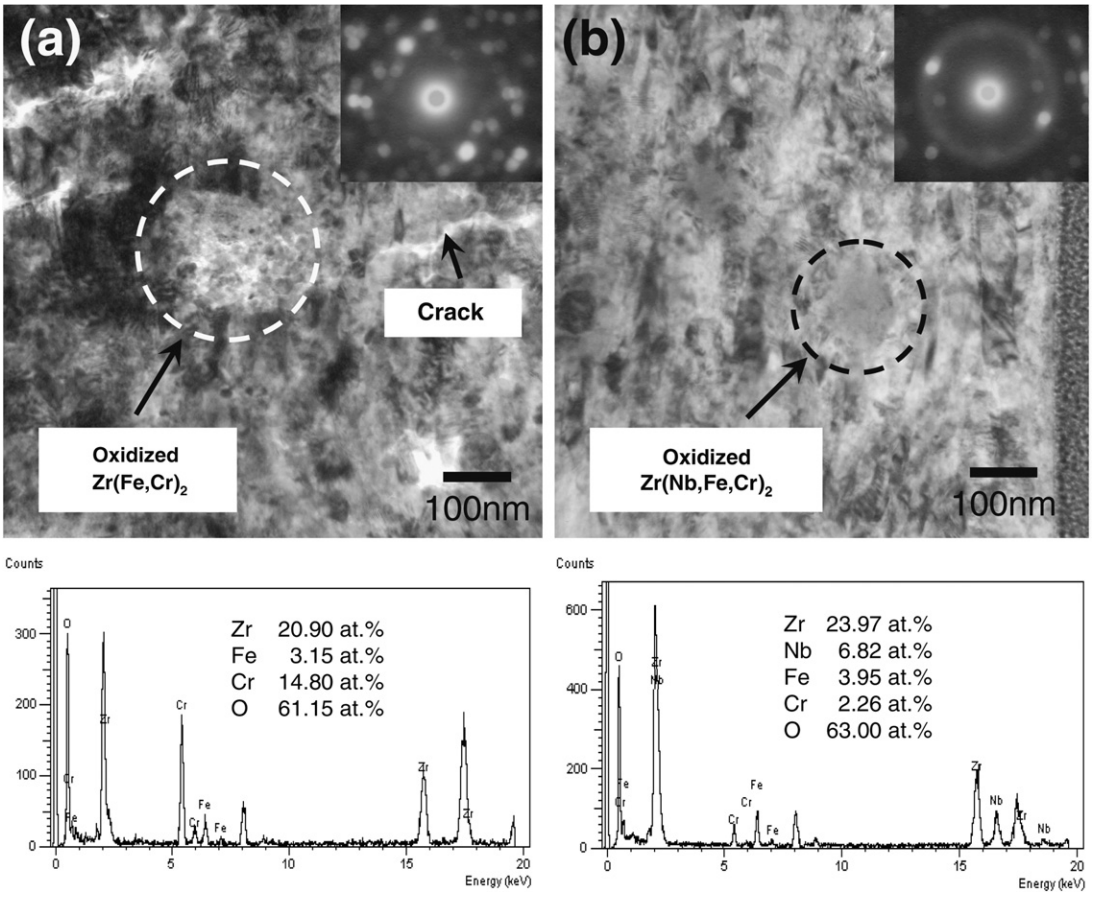

Fig. 7. TEM bright field images, the selected area diffraction patterns and the EDS spectra on (a) $Zr(Fe,Cr)_2$ at 3.5 μm away from the oxide/metal interface of Zircaloy-4 and (b) $Zr(Nb,Fe,Cr)_2$ at 3.5 μm away from the oxide/metal interface of HANA-4 corroded in 360 °C pure water for 1020 days.

that the excellent corrosion resistance of HANA-4 is partly attributed to the oxidation behavior of the precipitates.

3.6. Oxide protectiveness in LiOH solution

A great number of hypotheses have been proposed to explain the mechanism of a corrosion acceleration of Zircaloy-4 in LiOH solution. It has been reported that the substitution of Li^+ for Zr^{4+} causes excessive oxygen vacancies in an oxide and thereby enhances the diffusion rate of the oxygen ions through the oxide layer [16]. However, this is not appropriate when we consider that the diffusion rate through the grain boundary is 10^4 times faster than the bulk diffusion which was controlled by the concentration of the oxygen vacancies [17]. Therefore, it is more rational to establish a reason for the corrosion acceleration in LiOH solution in terms of its impact on the oxide grain morphology and the degree of the porosity.

Ramasubramanian et al. proposed that Zr–OLi groups are formed from the undissociated LiOH and retard the normal recrystallization processes of the oxide crystallites leading to a higher grain boundary area [18]. Such an effect would be increased with an increase of the oxide porosity since Li^+ or LiOH can penetrate more easily into the porous oxide. In this study, a layered structure was not observed in the oxide of Zircaloy-4 corroded in LiOH solution, as shown in Fig. 4(b). This is likely to be caused by the fact that Li^+ or LiOH promoted the formation of equiaxed grains rather than a periodic change of the grain morphology and thereby increased the corrosion rate.

Moreover, $Zr(Fe,Cr)_2$ is likely to be oxidized more readily in LiOH solution than in pure water after it is incorporated into the oxide. As shown in Fig. 8(a), $Zr(Fe,Cr)_2$ was oxidized at about 200 nm from the interface. This would imply that the oxide of Zircaloy-4 was not protective even in the interface region in LiOH solution. However, β-Nb at 200 nm from the interface of HANA-4 was not oxidized as shown in Fig. 8(b). The oxide formed on HANA-4 was revealed to be very protective against a diffusion of the oxygen ions in pure water. The oxide protectiveness of HANA-4 might be also effective in maintaining a lower corrosion rate even in LiOH solution. This seems to demonstrate that the oxide of HANA-4 was protective enough to prevent Li^+ or LiOH from penetrating into the oxide/metal interface.

4. Conclusion

Corrosion behavior of Zr–1.5Nb–0.4Sn–0.2Fe–0.1Cr (HANA-4) and Zircaloy-4 was investigated in 360 °C pure water and in 360 °C water containing 70 ppm Li. HANA-4 showed a much better corrosion resistance than Zircaloy-4 in pure water and maintained a lower corrosion rate even

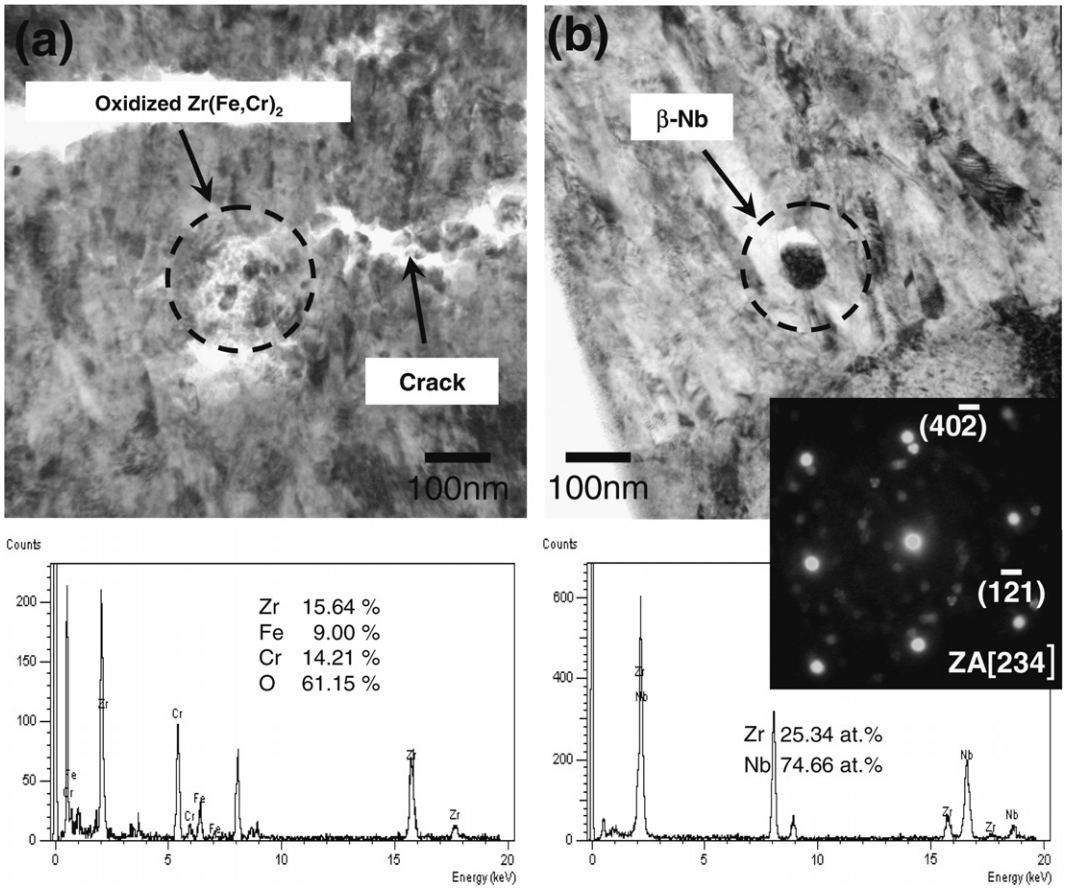

Fig. 8. TEM bright field images, the selected area diffraction patterns and the EDS spectra on (a) $Zr(Fe,Cr)_2$ at 200 nm away from the oxide/metal interface of Zircaloy-4 and (b) β-Nb at 200 nm away from the oxide/metal interface of HANA-4 corroded in 360 °C water containing 70 ppm Li for 830 days.

in LiOH solution where Zircaloy-4 showed an accelerated corrosion behavior. The oxide was characterized by an optical microscopy and a transmission electron microscopy. The oxide formed on HANA-4 in pure water was observed to have a layered structure with a smaller total oxide thickness for the same corrosion period, a higher layer thickness and a larger columnar grain size in the interface region when compared to Zircaloy-4. The oxide protectiveness of HANA-4 was also effective in maintaining a lower corrosion rate even in LiOH solution where a layered structure was not developed in the oxide of Zircaloy-4. This demonstrates that the oxide of HANA-4 was protective enough to prevent it from becoming porous by an ingress of Li^+ or LiOH.

Acknowledgements

This study was supported by KOSEF and MOST, Korean government, through its National Nuclear Technology Program.

References

[1] Y.H. Jeong, S.Y. Park, M.H. Lee, B.K. Choi, J.H. Baek, J.Y. Park, J.H. Kim, H.G. Kim, J. Nucl. Sci. Tech. 43 (2006) 977.
[2] G.P. Sabol, J. ASTM Int. 2 (2005) Paper ID JAI12942.
[3] P. Bossis, D. Pecheur, K. Hanifi, J. Thomazet, M. Blat, J. ASTM Int. 3 (2006) Paper ID JAI12404.
[4] J.Y. Park, B.K. Choi, S.J. Yoo, Y.H. Jeong, J. Nucl. Mater. 359 (2006) 59.
[5] K. Takeda, H. Anada, ASTM STP 1354 (2000) 592.
[6] M. Parise, O. Sicardy, G. Cailletaud, J. Nucl. Mater. 256 (1998) 35.
[7] A. Yilmazbayhan, A.T. Motta, R.J. Comstock, G.P. Sabol, R. Lai, Z. Cai, J. Nucl. Mater. 324 (2004) 6.
[8] A.T. Motta, A. Yilmazbayhan, R.J. Comstock, J. Partezana, G.P. Sabol, B. Lai, Z. Cai, J. ASTM Int., 2 (2005) Paper ID JAI 12375.
[9] J.S. Bryner, J. Nucl. Mater. 82 (1979) 84.
[10] D. Pecheur, V.P. Filippov, A.B. Bateev, J.J. Ivanov, ASTM STP 1423 (2002) 135.
[11] O. Gebhardt, A. Hermann, G. Bart, H. Blank, F. Garzarolli, I.L.F. Ray, ASTM STP 1295 (1996) 218.
[12] R.J. Comstock, G. Schoenberger, G.P. Sabol, ASTM 1295 (1996) 710.
[13] D. Pecheur, F. Lefebvre, A.T. Motta, C. Lemaignan, D. Charquet, ASTM STP 1245 (1994) 687.
[14] H. Anada, B.J. Herb, K. Nomoto, S. Hagi, R.A. Graham, T. Kuroda, ASTM STP 1295 (1996) 74.
[15] Y.P. Lin, O.T. Woo, J. Nucl. Mater. 277 (2000) 11.
[16] E. Hillner, J.N. Chirigos, WAPD-TM6307, Westinghouse Electric Corp., Bettis Atomic Laboratory, Pittsburgh, PA, USA, 1962.
[17] B. Cox, C. Roy, Electrochem. Tech. 4 (1966) 121.
[18] N. Ramasubramanian, N. Precoanin, V.C. Ling, ASTM STP 1023 (1989) 187.